# Synthesis of Ni-Fe thin films by electrochemical deposition technique and characterization of their microstructures and surface morphologies

UMUT SARAÇ

MALİK KAYA

MEVLANA CELALETTİN BAYKUL

# Synthesis of Ni-Fe thin films by electrochemical deposition technique and characterization of their microstructures and surface morphologies

**Umut SARAÇ**[1], **Malik KAYA**[2,*], **M. Celalettin BAYKUL**[3]

[1]Department of Science Education, Faculty of Education, Bartın University, Bartın, Turkey

[2]Vocational School of Health Services, Eskişehir Osmangazi University, Eskişehir, Turkey

[3]Department of Metallurgical and Materials Engineering, Faculty of Engineering, Eskişehir Osmangazi University, Eskişehir, Turkey

**Abstract:** Microstructural features and surface morphologies of Ni-Fe thin films fabricated by the electrochemical deposition technique have been experimentally studied. Ni-Fe thin films have been deposited under different deposition potentials and $FeSO_4$ concentrations. Energy dispersive X-ray measurements demonstrate that the Fe content decreases (increases) as the deposition potential ($FeSO_4$ concentration) is enhanced. All of the produced films exhibit an anomalous codeposition behavior. The effects of deposition potential and $FeSO_4$ concentrations on the degree of anomalous codeposition have been also characterized. X-ray diffraction studies reveal that the films have face-centered cubic crystallographic structures with [111] preferred crystallographic orientation regardless of the applied deposition conditions. However, the crystallization and the crystallite size of the films are affected by changing of the $FeSO_4$ concentration and the deposition potential. The results of scanning electron microscopy analyses verify that the surface structure of the film electroplated from the electrolyte with higher $FeSO_4$ concentration under higher deposition potential exhibits a more homogeneous and dense structure with smaller grain sizes.

**Key words:** Electrochemically fabricated Ni-Fe thin films, microstructure, morphology, deposition potential, $FeSO_4$ concentrations, anomalous codeposition

## 1. Introduction

Nickel-iron (Ni-Fe) alloy films with nanocrystalline structure have received great attention because of their good physical, magnetic, and mechanical features such as low coercive field, high magnetic permeability, and good corrosion resistance [1–5]. Because of these beneficial properties, Ni-Fe films with wide ranges of composition are utilized in various industrial and technological applications such as microelectrical mechanical systems, sensors, actuators, and magnetic recording devices [2,3,5,6]. Ni-Fe alloy thin films with both face-centered cubic (fcc) and body-centered cubic (bcc) can be fabricated by the electrochemical deposition technique, which has numerous unique advantages such as time efficiency, cost-effectiveness, low power consumption, and simplicity in controlling the deposition parameters when it is compared with the other high-vacuum techniques [1,7–9]. Ni-Fe thin films grown by electrochemical deposition technique exhibit anomalous codeposition behavior, since the less noble metal Fe is deposited preferentially compared to the more noble metal Ni [4,10]. In recent studies, as a special case of anomalous codeposition, anomalous codeposition that occurred inside the composition gradient

*Correspondence: malikkaya@ogu.edu.tr

zone near the substrate interface in electrochemically deposited Ni-Fe thin films with different thicknesses ranging between 5 and 500 nm was revealed and explained [11] and the magnetic and the microstructural properties in dependence of film thickness were also investigated [12].

The morphologies, chemical compositions, and magnetic and microstructural features of films fabricated by electrochemical deposition technique strongly depend on experimental parameters such as substrate type, metal ion concentrations in the electrolyte solution, applied cathode potential, and electrolyte pH. Indium tin oxide (ITO)-coated glasses are often preferred as a substrate in the electrochemical deposition technique due to their favorable properties including high transparency and sufficient conductivity [13–18]. It was shown that the magnetic features, surface morphologies, and structural properties of Ni-Fe films electrochemically deposited on ITO glass substrates are significantly affected by the $NiSO_4/FeSO_4$ molar ratio and pH value of the electrolyte solution [7]. A study also reported the effect of film thickness on the structural properties, morphology, domain structure, and FMR spectra in electrochemically deposited Ni-Fe films on ITO conducting glasses [19].

In this study, Ni-Fe thin films with different compositions were successfully fabricated onto ITO-coated glass substrates by electrochemical deposition technique from sulfate-based electrolyte solutions to investigate the compositional variation, microstructure, and surface morphology depending on the applied deposition potential and $FeSO_4$ concentration in the electrolyte. The results revealed that the properties are changed significantly by changing both deposition potential and $FeSO_4$ concentration.

## 2. Materials and methods

Ni-Fe alloy thin films were deposited by using the electrochemical deposition technique from sulfate-based electrolytes. All deposition processes were carried out in a conventional three-electrode cell consisting of counter, working, and reference electrodes using a potentiostat/galvanostat (VersaSTAT 3). A platinum wire as a counter electrode, ITO-coated glass substrate with a working area of about 1 cm$^2$ as a working electrode, and a saturated calomel electrode (SCE) as a reference electrode were used during electrochemical deposition of the films. The films were electrochemically deposited at three different deposition potentials of –1.2, –1.4 and –1.6 V vs. SCE from an electrolyte solution composed of 0.075 M $NiSO_4$, 0.0075 M $FeSO_4$, and 0.1 M $H_3BO_3$ without stirring. Subsequently, Ni-Fe thin films were fabricated at a constant deposition potential of –1.2 V vs. SCE from the electrolyte solutions with 0.075 M $NiSO_4$, 0.1 M $H_3BO_3$, and three different $FeSO_4$ concentrations of 0.0025, 0.0050, and 0.0075 M. All of the experiments were carried out at ambient temperature. In the experimental process, Ni-Fe films were also electrochemically deposited from an electrolyte having 0.0100 M $FeSO_4$ concentration at a constant deposition potential of –1.2 V vs. SCE and from an electrolyte consisting of 0.0075 M $FeSO_4$ concentration at a constant deposition potential of –1 V vs. SCE. However, the films could not be successfully fabricated under these electroplating conditions owing to their brittle features. The purpose of the addition of boric acid into electrolyte solution containing Fe and Ni ions is to improve the film quality and obtain stable pH during the electroplating process. Deionized (DI) water was utilized to prepare electrolyte solutions. Before the electrochemical deposition process, the surface of the substrates was cleaned in acetone solution for 10 min followed by 10 min in ethanol solution, and finally they were rinsed ultrasonically in DI water for 15 min. The film thickness was controlled by charge and it was kept at approximately 350 nm by adjusting the electroplating time based on Faraday's law for all applied deposition potentials and $FeSO_4$ concentrations. All electrolyte solutions used for the deposition of Ni-Fe thin films were freshly prepared.

In order to obtain knowledge about the crystallographic structure of the films, X-ray diffraction (XRD) measurements (Rigaku SmartLab) were performed with an XRD diffractometer (Cu K$\alpha$ radiation, $\lambda = 0.154059$

nm) by scanning in the $2\theta = 40°$–$55°$ range with 0.01 steps. To investigate the effect of the $FeSO_4$ concentration in the electrolyte and deposition potential on the surface morphological structure of the films a scanning electron microscope (SEM) (Tescan MAIA3) was used. The compositional analysis of the films was done with the SEM equipped for energy dispersive X-ray (EDX). All compositions mentioned in this study are given in atomic units (at.%). The electrolyte solution utilized for electrochemical deposition of the Ni-Fe thin films at different cathode potentials was characterized by the cyclic voltammetry (CV) technique. The scan was performed from +2 V to –1.8 V vs. SCE in the cathodic direction with a potential sweep rate of 20 mV/s. The film growth was also followed by recording the transient curves in all electroplating processes carried out under different $FeSO_4$ concentrations and applied deposition potentials.

## 3. Results and discussion

Ni-Fe thin films were electrochemically deposited on ITO from sulfate-based electrolytes at ambient temperature without stirring. The aim of the study was to fabricate Ni-Fe thin films in two different procedures and investigate the effects of changing the deposition potential and $FeSO_4$ concentration on the film composition, the surface morphology, and the microstructure. To determine suitable cathode potentials for electrochemical deposition of Ni-Fe thin films on ITO substrates, the CV technique was applied for the electrolyte composed of 0.075 M $NiSO_4$, 0.0075 M $FeSO_4$, and 0.1 M $H_3BO_3$ utilized for film growth at different deposition potentials. Figure 1 demonstrates the CV curve of the aqueous solution. A broad peak appears at positive potentials on the anodic branch (see Figure 1). This peak probably appears due to the dissolution of the Fe ions as it was reported that the dissolution peak of Ni ions does not appear in the CV curve of an electrolyte having only Ni ions in the potential regions on the anodic branch [20,21]. On the cathodic branch, the current density rises with increasing cathode potential after the deposition potential of about –0.8 V. At this point, Ni and Fe ions begin to deposit on the ITO. Consequently, the findings acquired from the CV curve suggest that the cathode potential should be over about –0.8 V vs. SCE for electroplating of Ni-Fe on ITO substrates. Hence, in this research, potentials in the range between –1.2 and –1.6 V vs. SCE were chosen for electrochemical deposition of Ni-Fe thin films by looking at their appearance.

To observe the first 50-s growth period of the Ni-Fe thin films, the transient curves were also recorded. Figure 2 shows the transient curves of Ni-Fe thin films fabricated at different deposition potentials and $FeSO_4$ concentrations. The current density is almost stable during the deposition of the films in both different deposition potentials and different $FeSO_4$ concentrations. This shows that Ni-Fe thin films are uniformly electrodeposited on ITO-coated glass substrates. However, the current density slightly increases to a higher value when the $FeSO_4$ concentrations in the electrolyte increase. The current density also increases with increasing deposition potential.

EDX results of Ni-Fe thin films fabricated at different deposition potentials and $FeSO_4$ concentrations are given in the Table. The Fe content slightly decreases in the film composition when the deposition potential increases from –1.2 to –1.6 V vs. SCE (Table). The decrease of Fe content with increasing deposition potential was also revealed in Ni-Fe coatings electrochemically fabricated at different applied current densities [22] and deposition potentials [23]. It was also determined that as Fe content increases, Ni content consequently decreases with increasing $FeSO_4$ concentrations in the electrolyte. On the other hand, the ratio of Ni/Fe in all fabricated Ni-Fe thin films was determined to be lower than the molar ratio of $NiSO_4$/$FeSO_4$ in the electrolyte solution, as shown in Figure 3. Nickel should be deposited more than iron, because nickel is a more noble metal than iron. However, EDX results show that the less noble metal iron is deposited more than Ni in Ni-Fe thin
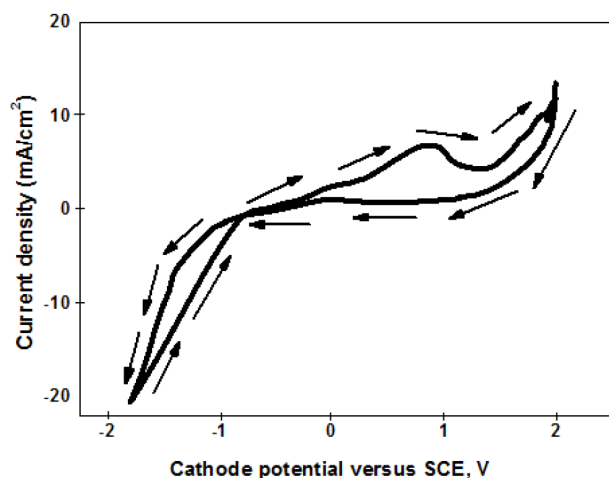
**Figure 1.** The CV curve of the electrolyte solution utilized for electroplating of Ni-Fe thin films onto ITO-coated glass substrates at different deposition potentials.
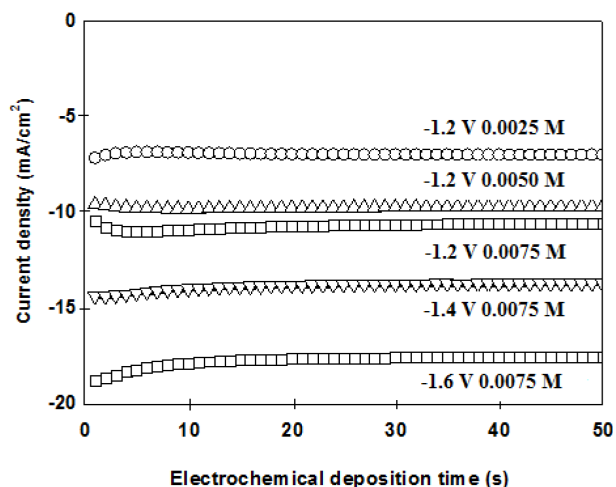


**Figure 2.** The transient curves of Ni-Fe thin films electrochemically deposited at different deposition potentials and $FeSO_4$ concentrations.

films regardless of deposition potential and $FeSO_4$ concentrations. This can be attributed to the anomalous codeposition behavior in the electrochemical deposition of Ni-Fe thin films. Anomalous codeposition was also reported in electrochemically deposited Ni-Fe thin films on ITO-coated glass substrates [7]. The evolution of the ratio of Ni/Fe in the films according to $NiSO_4/FeSO_4$ molar ratio in the electrolyte adjusted by changing $FeSO_4$ concentrations is demonstrated in Figure 3a. As shown Figure 3a, the ratio of Ni/Fe in the films increases linearly with increasing $NiSO_4/FeSO_4$ molar ratio in the electrolyte. This may reflect that the degree of anomalous codeposition behavior is not influenced by the $FeSO_4$ concentration in the electrolyte. The change observed in the Ni/Fe ratio within the films with respect to deposition potential is shown in Figure 3b. The degree of anomalous codeposition behavior is lower in the higher applied cathode potentials.
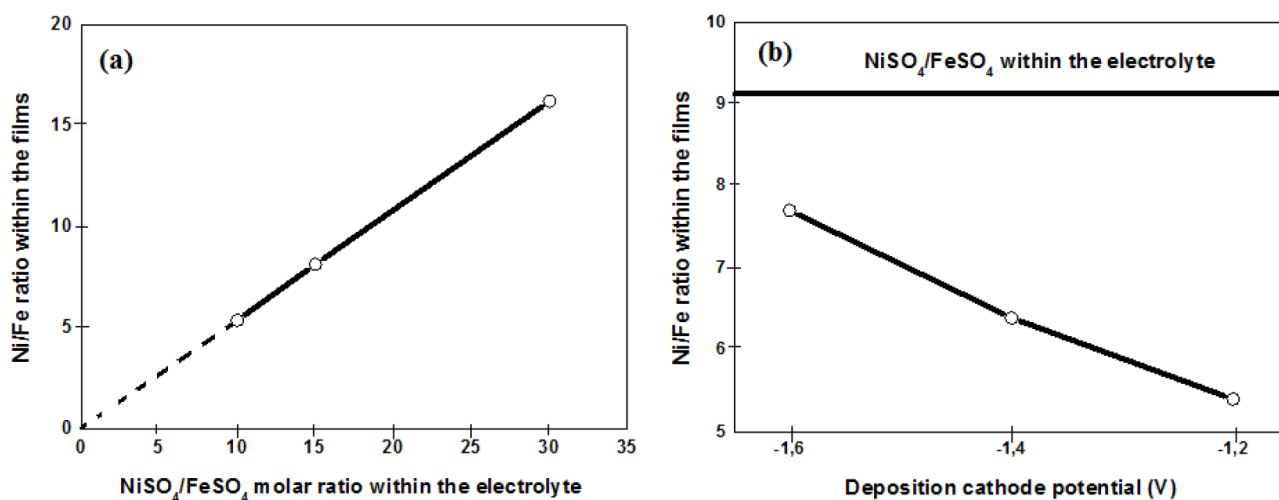


**Figure 3.** The evolution of Ni/Fe ratio in the films as a function of a) $NiSO_4/FeSO_4$ molar ratio in the electrolytes and b) deposition potential.

**Table.** The change of chemical composition, lattice parameter, and crystallite size depending on the deposition potential and $FeSO_4$ concentration.

| Deposition (V) | potential (M) | FeSO4 film composition | | Lattice parameter (nm) | Crystallite size (nm) |
|---|---|---|---|---|---|
| | | Fe (at.%) | Ni (at.%) | | |
| 1.2 | 0.0025 | 5.8 | 94.2 | 0.35364 | 26.8 |
| 1.2 | 0.0050 | 10.9 | 89.1 | 0.35413 | 21.7 |
| 1.2 | 0.0075 | 15.6 | 84.4 | 0.35454 | 16.0 |
| 1.4 | 0.0075 | 13.5 | 86.5 | 0.35442 | 18.2 |
| 1.6 | 0.0075 | 11.4 | 88.6 | 0.35419 | 19.0 |

XRD results of Ni-Fe thin films deposited at different deposition potentials and $FeSO_4$ concentrations are shown in Figure 4. All of the fabricated Ni-Fe thin films have diffraction peaks related to fcc phase structure, as seen in Figure 4, indicating that fcc solid solutions are formed. The bcc peaks for bulk Fe are not observed in the XRD patterns. The nonexistence of bcc Fe peaks can be attributed to the content of Fe being less than 15.6% in the film structure. The phase structure of Ni-Fe films electroplated from both chloride- and sulfate-based electrolyte solutions is fcc for Fe content within the film of <50% [24].
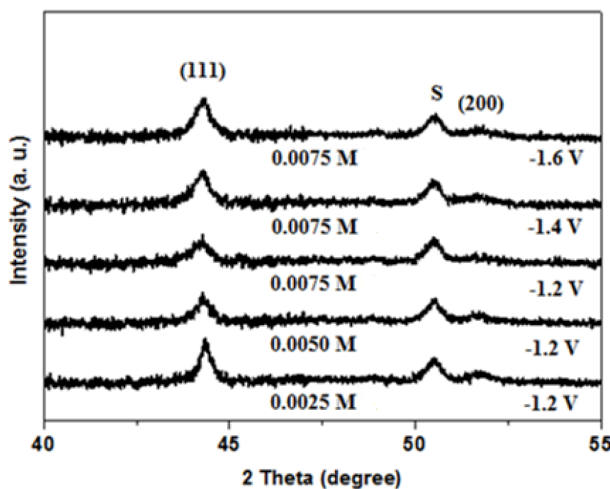


**Figure 4.** XRD patterns of Ni-Fe thin films fabricated under various deposition potentials and $FeSO_4$ concentrations. The peak demonstrated by S appears due to the ITO substrate.

As seen from Figure 4, the width of the (111) peaks decreases when the deposition potential increases. Oppositely, the peak widths increase with increasing $FeSO_4$ concentrations, resulting in a change in the crystallite size. The crystallite size of Ni-Fe thin films for the fcc (111) peak was calculated by the Scherrer formula [25] as a function of the deposition potential and the $FeSO_4$ concentrations in the electrolyte. The change of the crystallite size depending on deposition potential and $FeSO_4$ concentrations is given in the Table. The crystallite size of Ni-Fe thin films is obtained between 16.0 and 26.8 nm, which demonstrates that the Ni-Fe thin films have crystallites of nanometer scale. As clearly seen from the Table, an increase in the deposition potential resulted in an increase in the size of crystallites from 16.0 to 19.0 nm. An increase in the size of crystallites with increasing deposition potential was also observed in previous works and the reason for that was also discussed [26–30]. On the contrary, whenever $FeSO_4$ concentrations in the electrolyte increased, the size of crystallites significantly reduced from 26.8 to 16.0 nm. This decrement achieved in the crystallite size with the increase of Fe content is in good agreement with the results of previous studies [31,32]. According to

findings obtained in the present study, it may be said that the $FeSO_4$ concentration plays a more effective role than deposition potential on the size of crystallites of Ni-Fe thin films.

It is also observed that the crystallization of the films is affected directly by the experimental conditions. The peak intensities increase with increasing deposition potential, which can also represent an increment in the crystallite size of films. In opposition to that, the peak intensities decrease with increasing $FeSO_4$ concentrations in the electrolyte, with consequent rising of Fe content in the films as seen from Figure 4, which can also reflect a decrement in the crystallite size of films. Thus, it may be concluded that the crystallization of the films decreases with the increase of $FeSO_4$ concentrations and increases with increasing deposition potential due to change of film composition. In addition to that, in all cases the intensity of the (200) diffraction peak was determined to be extremely low in comparison with the (111) one. From the XRD analyses, it is also observed that there is no transition in either phase structure or preferred crystallographic orientation. Thus, it can be concluded that all of the films exhibit the fcc phase structure with (111) preferred crystallographic orientation.

Structural analyses show that the position of the fcc (111) peak shifted to a smaller angle with increasing $FeSO_4$ concentrations in the electrolyte, but shifted to a greater angle with increase of the deposition potential. This gives rise to change of the lattice parameter. The lattice parameters of Ni-Fe thin films were calculated from the XRD patterns for the fcc (111) peaks as a function of the $FeSO_4$ concentrations and the deposition potential using Bragg's law. As shown in the Table, the lattice parameter of the fcc (111) peak enhances with the increase of $FeSO_4$ concentrations in the electrolyte. This increase can be attributed to an increase of $FeSO_4$ concentrations in the electrolyte, resulting in an increase of Fe content in the film structure. An enhancement revealed in the lattice parameter with the Fe content was also reported in fcc structure Ni-Fe films [1,33] and also in fcc structure Ni-Cu-Fe thin films [13]. However, the lattice parameter of the fcc (111) peak decreases with increase of the deposition potential. This decrease can be ascribed to the decrease of Fe content in the film structure with increasing of the deposition potential, since the lattice parameter of fcc Fe is higher than that of fcc Ni [34].

Figures 5a and 5b display the SEM images of Ni-Fe thin films fabricated at a constant deposition potential of −1.2 V vs. SCE, but in the electrolyte solutions with low (0.0025 M) and high (0.0075 M) $FeSO_4$ concentrations, respectively. The surface morphologies are significantly affected by changing $FeSO_4$ concentrations. As seen from Figure 5, surfaces of Ni-Fe thin films fabricated in different electrolyte solutions containing different $FeSO_4$ concentrations are formed with different size grains and exhibit crack-free morphology and granular structure. The grain boundaries of the film with low Fe content fabricated from the electrolyte with low $FeSO_4$ concentrations are more prominent, as seen in Figure 5a. However, the film surface has a more homogeneous and dense structure when the $FeSO_4$ concentration is high, as shown in Figure 5b. The average grain size decreases with increasing $FeSO_4$ concentrations. The average size of grains is around 300 and 200 nm for low and high $FeSO_4$ concentrations, respectively. This finding for grain size with increasing $FeSO_4$ concentrations in the electrolyte was also observed in Ni-Fe films electrochemically deposited on an ITO substrate from electrolytes with various $NiSO_4/FeSO_4$ molar ratios under different deposition conditions [7] and Ni-Cu-Fe thin films electrochemically fabricated from electrolytes with different $FeSO_4$ concentrations on an ITO substrate [13].

Figures 6a and 6b show the low and high magnification of SEM images of Ni-Fe thin film electrochemically deposited from the electrolyte with 0.0075 M (high) $FeSO_4$ concentrations under high deposition potential of −1.6 V vs. SCE, respectively. An improvement in the compactness and homogeneity of surface structure is revealed at high deposition potential. The surface morphology of this film is still granular, consisting of grains
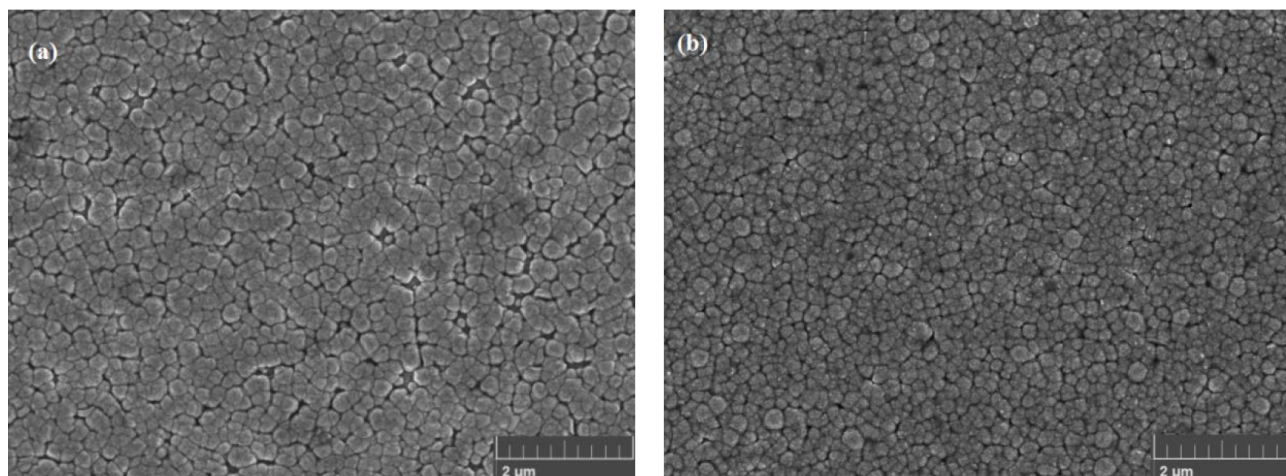
**Figure 5.** SEM images of Ni-Fe thin films electroplated at low deposition potential of –1.2 V vs. SCE from the electrolytes with different $FeSO_4$ concentrations: a) 0.0025 M $FeSO_4$ (94.2 at.% Ni-5.8 at.% Fe) and b) 0.0075 M $FeSO_4$ (84.4 at.% Ni-15.6 at.% Fe).

with smaller sizes compared to other films. The average size of these grains appearing on the film surface fabricated at high deposition potential of –1.6 V vs. SCE is around 100 nm. Similar evolution in grain size with increasing deposition potential was also detected in electrochemically deposited Ni-Fe films on Cu substrates [9], Ni-Co [29], Fe-Cu [35], and Ni-Fe-Cu [30] thin films on ITO substrates under different applied current densities. A decrement in the grain size achieved by increasing both deposition potential and $FeSO_4$ concentrations in the electrolyte may be attributed to more developed nucleation sites on the surface of ITO during the electroplating process of the films. An enhancement in both deposition potential and $FeSO_4$ concentration in the electrolyte may lead to an increment in the nucleation rate. Hence, smaller grains appear on the film surfaces and the films exhibit more dense structure at the higher deposition potential and higher $FeSO_4$ concentrations.
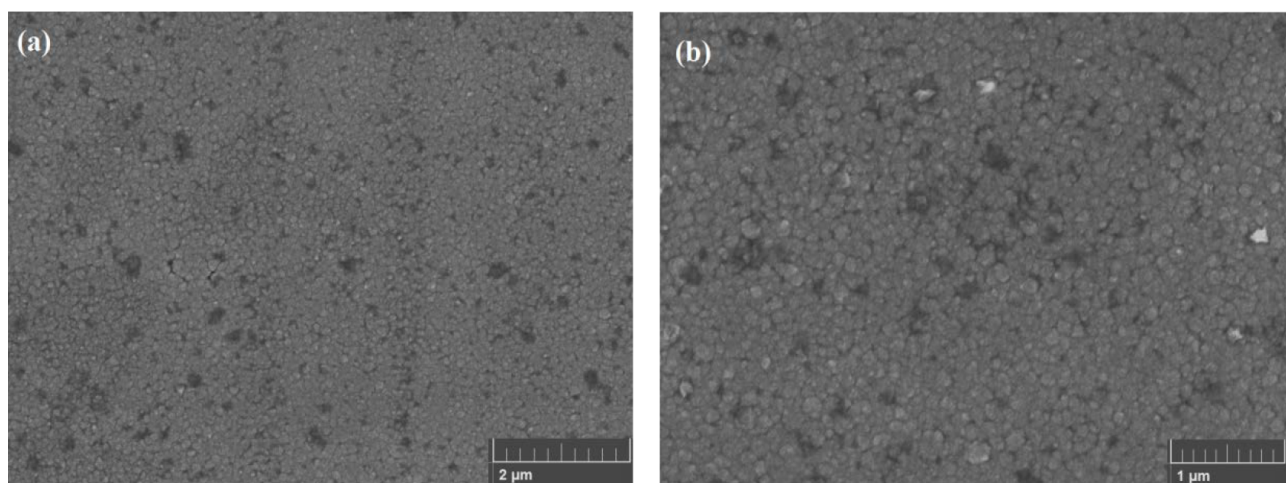


**Figure 6.** SEM images of Ni-Fe thin film with 88.6 at.% Ni and 11.4 at.% Fe electrochemically deposited from the electrolyte having 0.0075 M $FeSO_4$ at high deposition potential of –1.6 V vs. SCE at a) low and b) high magnification.

## 4. Conclusions

Ni-Fe thin films with different compositions have been successfully electroplated onto ITO-coated glass substrates at three different deposition potentials of –1.2, –1.4, and –1.6 V vs. SCE and three different $FeSO_4$ concentrations of 0.0025, 0.0050, and 0.0075 M at a constant deposition potential of –1.2 V vs. SCE. Compositional analyses reveal that the increase of Fe content in the film structure is consistent with the increase of $FeSO_4$ concentration in the electrolyte. However, by increasing the deposition potential, the Fe content is slightly decreased. Less noble Fe is always preferentially deposited in this work under all conditions, which can be explained by the anomalous codeposition behavior of Ni-Fe. The degree of anomalous codeposition is not changed by changing the $FeSO_4$ concentration in the electrolyte, but it is reduced by increasing the deposition potential. All of the fabricated films exhibit fcc phase structure with (111) preferred crystallographic growth orientation. However, a decrement (an increment) in the crystallization is revealed with the increase of $FeSO_4$ concentrations (deposition potential). The crystallite size is slightly increased from 16.0 to 19.0 nm by increasing the deposition potential and considerably reduced from 26.8 to 16.0 nm as the $FeSO_4$ concentration in the electrolyte is enhanced. The SEM results show that the surface morphologies of electrochemically fabricated Ni-Fe thin films exhibit a granular structure. The film electroplated from the electrolyte with higher $FeSO_4$ concentrations under higher deposition potential has a more homogeneous and dense structure consisting of smaller grains.

## Acknowledgment

## References

[1] Li, H.; Ebrahimi, F. *Mater. Sci. Eng. A* **2003**, *347*, 93-101.

[2] Myung, N. *Bull. Korean Chem. Soc.* **2001**, *22*, 994-998.

[3] Phua, L. X.; Phuoc, N. N.; Ong, C. K. *J. Alloys Compd.* **2012**, *520*, 132-139.

[4] Nakano, H.; Matsuno, M.; Oue, S.; Yano, M.; Kobayashi, S.; Fukushima, H. *Mater. Trans.* **2004**, *45*, 3130-3135.

[5] Torabinejad, V.; Aliofkhazraei, M.; Assareh, S.; Allahyarzadeh, M. H.; Sabour Rouhaghdam, A. *J. Alloys Compd.* **2017**, *691*, 841-859.

[6] Hou, X.; Liu, S.; Li, J.; Yang, S.; Guo, B. *Mater. Manufact. Process.* **2016**, *31*, 62-66.

[7] Su, X.; Qiang, C. *Bull. Mater. Sci.* **2012**, *35*, 183-189.

[8] Subramanian, B.; Govindan, K.; Swaminathan, V.; Jayachandran, M. *Trans. Inst. Metal Finish.* **2009**, *87*, 325-329.

[9] Cao, Y.; Wei, G. Y.; Ge, H. L.; Meng, X. F. *Surf. Eng.* **2014**, *30*, 97-101.

[10] Brenner, A. *Electrodeposition of Alloys Principles and Practice*; Academic Press: New York, NY, USA, 1963.

[11] Tabakovic, I.; Gong, J.; Riemer, S.; Kautzky, M. *J. Electrochem. Soc.* **2015**, *162*, D102-D108.

[12] Gong, J.; Riemer, S.; Kautzky, M.; Tabakovic, I. *J. Magn. Magn. Mater.* **2016**, *398*, 64-69.

[13] Sarac, U.; Baykul, M. C. *J. Mater. Sci. Mater. Electron.* **2014**, *25*, 2554-2560.

[14] Nzoghe-Mendome, L.; Ebothé, J; Aloufy, A.; Kityk, I. V. *J. Alloys Compd.* **2008**, *459*, 232-238.

[15] Nzoghe-Mendome, L.; Aloufy, A.; Ebothé, J.; Hui, D.; El Messiry, M. *Mater. Chem. Phys.* **2009**, *115*, 551-556.

[16] Roca i Cabarrocas, R.; Chévrier, J. B.; Huc, J.; Lloret, A.; Parey, J. Y.; Schmitt, J. P. M. *J. Vac. Sci. Technol. A* **1991**, *9*, 2331-2341.

[17] Ebothé, J. *J. Appl. Phys.* **1995**, *77*, 233-239.

[18] Sarac, U.; Baykul, M. C. *J. Alloys Compd.* **2013**, *552*, 195-201.

[19] Cao, D.; Wang, Z.; Feng, E.; Wei, J., Wang, J.; Liu, Q. *J. Alloys Compd.* **2013**, *581*, 66-70.

[20] Karpuz, A.; Kockar, H.; Alper, M.; Karaagac, O.; Haciismailoglu, M. *Appl. Surf. Sci.* **2012**, *258*, 4005-4010.

[21] Kockar, H.; Alper, M.; Topcu, H. *Eur. Phys. J. B* **2004**, *42*, 497-501.

[22] Zhang, Y. H.; Ding, G. F.; Cai, Y. L.; Wang, H.; Cai, B. *Mater. Charact.* **2006**, *57*, 121-126.

[23] Kuru, H.; Kockar, H.; Alper, M.; Karaagac, O. *J. Magn. Magn. Mater.* **2015**, *377*, 59-64.

[24] Myung, N. V.; Nobe, K. *J. Electrochem. Soc.* **2001**, *148*, C136-C144.

[25] Wilson, A. J. C. *Proc. Phys. Soc. Lond.* **1962**, *80*, 286-294.

[26] Ebrahimi, F.; Ahmed, Z. *J. Appl. Electrochem.* **2003**, *33*, 733-739.

[27] Hassani, S. H.; Raeissi, K.; Golozar, M. A. *J. Appl. Electrochem.* **2008**, *38*, 689-694.

[28] Farzaneh, M. A.; Zamanzad-Ghavidel, M. R.; Raeissi, K.; Golozar, M. A.; Saatchi, A.; Kabi, S. *Appl. Surf. Sci.* **2011**, *257*, 5919-5926.

[29] Sarac, U.; Baykul, M. C.; Uguz, Y. *J. Supercond. Nov. Magn.* **2015**, *28*, 1041-1045.

[30] Sarac, U.; Kaya, M.; Baykul, M. C. *J. Phys. Conf. Ser.* **2016**, *766*, 012025.

[31] Cheung, C.; Djuanda, F.; Erb, U.; Palumbo, G. *Nanostruct. Mater.* **1995**, *5*, 513-523.

[32] Ma, I.; Zhang, I.; Li, X. B.; Li, Z. Y.; Zhou, K. C. *Trans. Nonferrous Metals Soc. China* **2015**, *25*, 146-153.

[33] Leith, S. D.; Ramli, S.; Schwartz, D. T. *J. Electrochem. Soc.* **1999**, *146*, 1431-1435.

[34] Nam, H. S.; Yokoshima, T.; Nakanishi, T.; Osaka, T.; Yamazaki, Y.; Lee, D. N. *Thin Solid Films* **2001**, *384*, 288-293.

[35] Sarac, U.; Baykul, M. C. *J. Mater. Sci. Technol.* **2012**, *28*, 1004-1009.